Hadronic final states at HERA

P. J. Bussey
for the H1 and ZEUS Collaborations

School of Physics and Astronomy, University of Glasgow, Glasgow
G12 8QQ, United Kingdom

Talk presented at the XXXVII International Conference on High Energy Physics, Valencia, Spain, 2-9 July, 2014

Abstract

Recent measurements of hadronic final states by H1 and ZEUS at HERA are presented. The H1 measurements consist of measurements of charged particle spectra in deep-inelastic *ep* scattering and of forward photons and neutrons. The ZEUS results consist of a series of measurements of prompt photons in photoproduction.

1 Introduction

This talk presents some recent measurements of hadronic final states from the H1 and ZEUS Collaborations at HERA. From H1, measurements of charged particle spectra in deep-inelastic scattering (DIS) and of forward photons and neutrons are shown. The ZEUS results consist of a series of measurements of prompt photons in photoproduction. More complete details of the theoretical models that are used can be found in the referenced papers and the citations therein.

2 Charged-particle spectra in deep-inelastic scattering

The H1 Collaboration have measured the distributions of charged particles in *ep* DIS, and compared the results with theoretical models [1]. The usual variables are used, namely the virtual photon virtuality Q^2 and y defined as the fractional energy loss of the lepton in the proton rest frame. The variable x is defined as Q^2/sy, and the variables are defined in the hadronic centre-of-mass frame. In this analysis (only), the $+Z^*$ axis is taken in the direction of the virtual photon. Charged-particle densities are integrated over the range $5 < Q^2 < 100$ GeV^2.

As Q^2 and x decrease, the evolution of the scattering process should change from a DGLAP to a BFKL mechanism. These form the basis of the theoretical models tested, and there is a further model, CCFM, which is a combination of these two approaches. The models differ in details concerning the transverse-momentum p_T ordering of the radiated partons in the calculations of the process. Also, RAPGAP uses DGLAP evolution, while DJANGOH uses a colour dipole model and a BFKL-like evolution, and CASCADE uses CCFM. The HERWIG model uses the POWHEG option.

The results show that none of the models tested agrees with the data very well over the entire measured p_T^* range. However DJANGOH does best. Further cross sections (not presented here) in bins of Q^2 and x show that at low p_T^* the distributions in η^* are satisfactorily described by all the models except CASCADE while at higher p_T^* values, none of the models is satisfactory except for DJANGOH.

3 Forward photons and neutrons

Positioned 106 m downstream of the interaction beyond some bending magnets, the H1 Forward Neutron Counter was able to detect and distinguish between very forward emerging photons and neutrons. Both types of particle emerged from the decay of excited proton states, while the neutrons were also produced through colour singlet exchange processes. The production rates of these particles were measured by H1, with a particular emphasis on establishing whether Feynman scaling holds, i.e. whether cross sections as a function of the centre-of-mass energy W are independent of the Feynman variable $x_F = 2p_{\|}^*/W$. The centre-of-mass energy W is defined as $\sqrt{ys - Q^2}$ and all variables are defined in the laboratory frame.

Measurements were made over the range $6 < Q^2 < 100$ GeV^2. Models tested included LEPTO, based on Lund string fragmentation, and RAPGAP combined with ARIADNE, which uses a colour dipole (CDM) formalism. A further set of theoretical calculations made use of models that were originally constructed to simulate cosmic ray showers, but were adapted for the ep context. These were SIBYLL and QGSJET, which are reggeon-based and were interfaced using PHOJET, and EPOS LHC, which is based on a parton model, modifying the treatment of central diffraction according to LHC measurements.

Figure 2 presents cross sections for forward photons, normalised relative to the inclusive DIS cross section, as a function of x_F, for three different ranges of W. It can be seen that the cross sections show no discernable

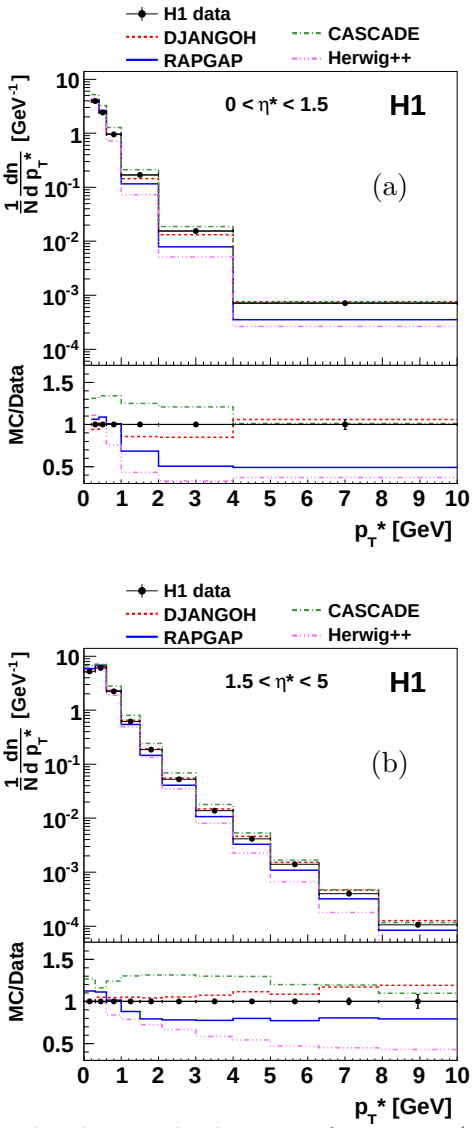

Figure 1: Normalised particle densities from H1: (a) for central pseudorapidities, (b) for forward pseudorapidities.

variation with W, confirming the principle of Feynman scaling. The colour dipole model does not fit well the shape of the distribution. The cosmic-ray based models show a better ability to fit the data, but SIBYLL fails. The absolute values of the normalised cross sections are not reproduced well by all the models. Figure 3 presents the corresponding neutron cross sections.

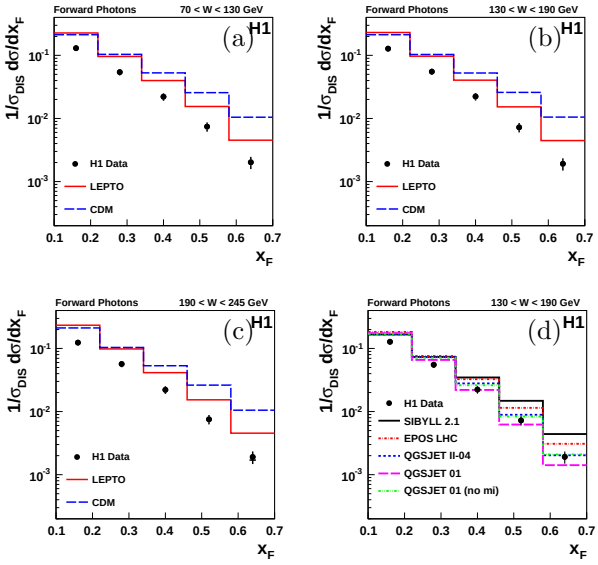

Figure 2: x_F distributions for forward photons in H1 for a series of different centre-or-mass ranges (a-c) compared to LEPTO and CDM, and an example (d) of comparisons to other models.

Feynman scaling is again confirmed, and a combination of RAPGAP and CDM effectively reproduces the shape and the absolute value of the normalised cross sections. Of the cosmic-ray based models, there is greater variability than with the photons, and only EPOS LHC can be considered reasonably satisfactory.

Figure 4 shows the total photon and neutron cross sections, normalised to the total DIS cross sections, for photons and neutrons respectively. Comparison is made to the cosmic-ray based models, showing that all are consistently high in the photon case, but vary widely in the neutron case with EPOS LHC being best. Both sets of data distributions are flat in W.

4 Isolated "prompt" photon production

The ZEUS Collaboration have performed studies of isolated high-energy photons, known as "prompt" photons, in photoproduction, measuring the basic photon and jet variables [3] and a number of other kinematic quantities [4]. The photons were detected in the electromagnetic section of the ZEUS Barrel Calorimeter, and jets were identified by "energy-flow objects"

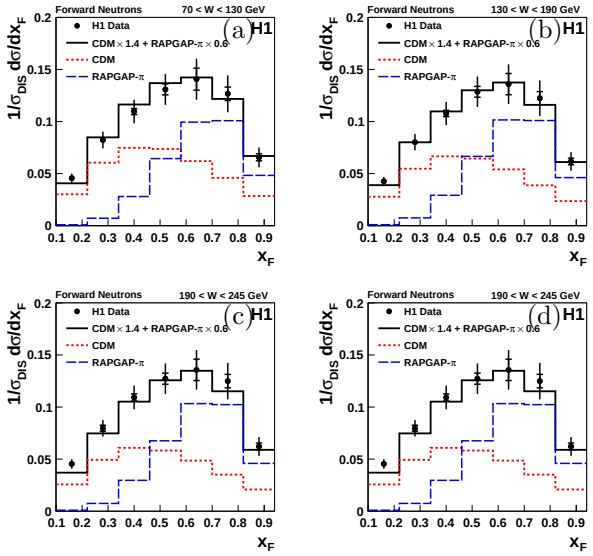

Figure 3: x_F distributions for forward neutrons in H1 for a series of different centre-or-mass ranges (a-c) compared to LEPTO and CDM, and an example (d) of comparisons to other models.

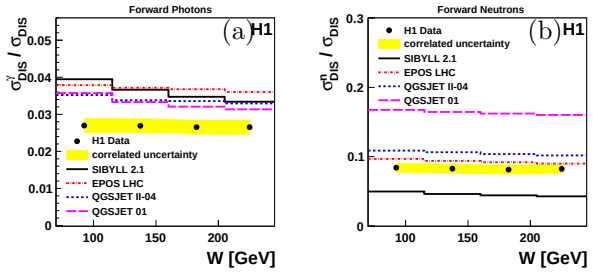

Figure 4: Normalised cross sections as a function of W for (a) forward photon production (b) forward neutron production, compared to a number of theoretical predictions.

constructed from calorimeter energy deposits and measured tracks. The photon signal was accompanied by a background arising from neutral hadrons such as π^0 and η mesons, which characteristically gave broader clusters of firing cells in the calorimeter. For each measured bin, a fit was performed to the width of the calorimeter cell cluster, so as to extract the photon signal.

Two theoretical models were tested. That of Fontannaz, Guillet and

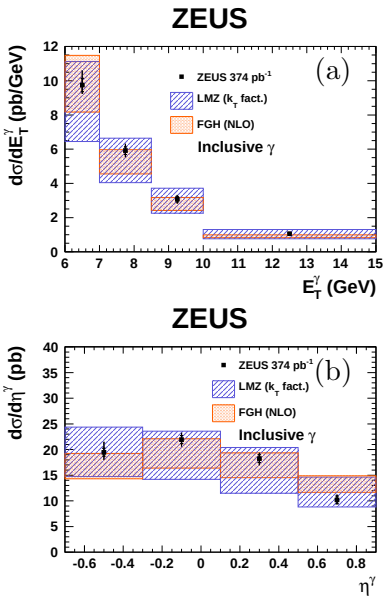

Figure 5: Distributions in (a) transverse energy and (b) pseudorapidity of inclusively produced isolated photons in ZEUS.

Heinrich (FGH) consisted of a standard next-to-leading-order QCD calculation augmented by a box diagram contribution and a jet fragmentation contribution. A second model, by Lipatov, Malyshev and Zotov (LMZ) used unintegrated parton distributions and an initial-state parton cascade.

Measurements were made for photon and jet transverse energies above 6 GeV and 4 GeV respectively. An important phenomenological quantity is $x_\gamma^{\rm meas}$, defined as the fraction of the final-state $E - p_Z$ that is contained in the photon and the jet, hence giving a relativistically-invariant measure of the fraction of the incoming photon energy that takes part in the QCD scattering process. In direct processes, all the photon energy takes part in the QCD scatter, while in resolved processes the photon acts as a source of partons. When measured, smearing due to fragmentation and higher-order processes becomes introduced. Cross sections were evaluated for the entire $x_\gamma^{\rm meas}$ range, and for ranges below and above a value of 0.8, which denoted resolved-enhanced and direct-enhanced regions of the kinematics. An isolation criterion is imposed, such that a photon must contain at least 90% of the energy of the jet-like object (which may be just the photon itself) that contains it. This reduces backgrounds and the effects of the fragmentation component, which is difficult to model accurately.

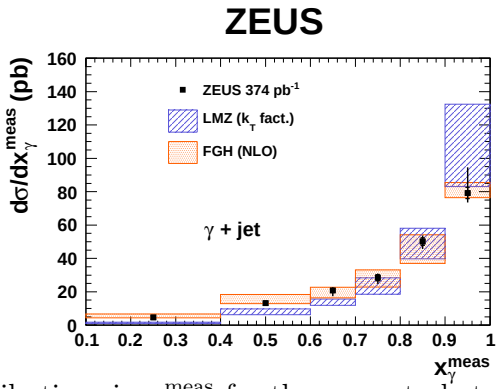

Figure 6: Distributions in $x_\gamma^{\rm meas}$ for the prompt-photon + jet final state in photoproduction.

Figure 5 presents cross sections for inclusive photons as functions of transverse energy and of pseudorapidity. Both the theoretical models give a good description of the distributions. The cross section in $x_\gamma^{\rm meas}$ is shown in fig. 6, where the enhancement towards the value of unity is due to the direct photoproduction process, while the resolved process gives a broader distribution. The theoretical FGH is in good agreement with the data, the LMZ model slightly less so.

For the second set of new measurements [4] an updated version of the LMZ calculation was used. The corresponding distributions when the photon is accompanied by a jet show good agreement with both models. Distributions for the transverse energy of the jet are given for the two $x_\gamma^{\rm meas}$ ranges in fig. 7 and show that while the direct-enhanced region is well-described by both models, the resolved-enhanced region has its pseudorapidity distribution poorly described by the LMZ model, possibly indicating a defect in the modelling of the initial-state parton cascade.

Figure 8 shows that the difference between the azimuths of the photon and the jet is well-described both by the parton-level models already mentioned, and also by the parton-shower Monte Carlos PYTHIA and HERWIG. This suggests that the showering mechanisms used in the latter are in some circumstances a good representation of a higher-order parton calculation.

5 Conclusions

The HERA experiments have continued to produce new and innovative measurements of hadronic final states, capable of testing state-of-the art theo-

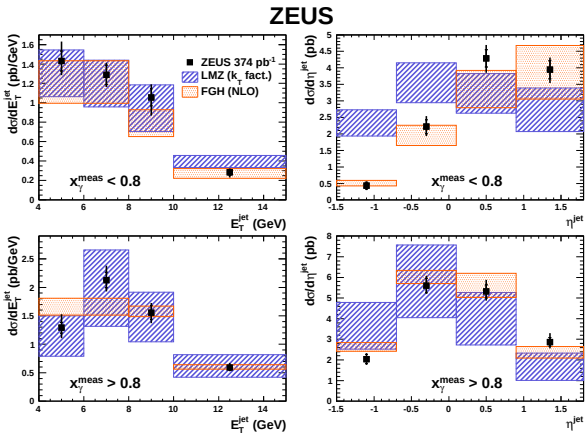

Figure 7: Distributions in jet transverse energy and pseudorapidity for $x_\gamma^{\rm meas}$ values less than and greater than 0.8

retical calculations. Further results are expected over the coming year.

References

[1] C. Alexa *et al.* [H1 Collaboration], Eur. Phys. J. C **73** (2013) 2406.

[2] V. Andreev *et al.* [H1 Collaboration], Eur. Phys. J. C **74** (2014) 2915.

[3] H. Abramowicz *et al.* [ZEUS Collaboration], Phys. Lett. B **730** (2014) 293.

[4] H. Abramowicz *et al.* [ZEUS Collaboration], JHEP 08 (2014) 023.

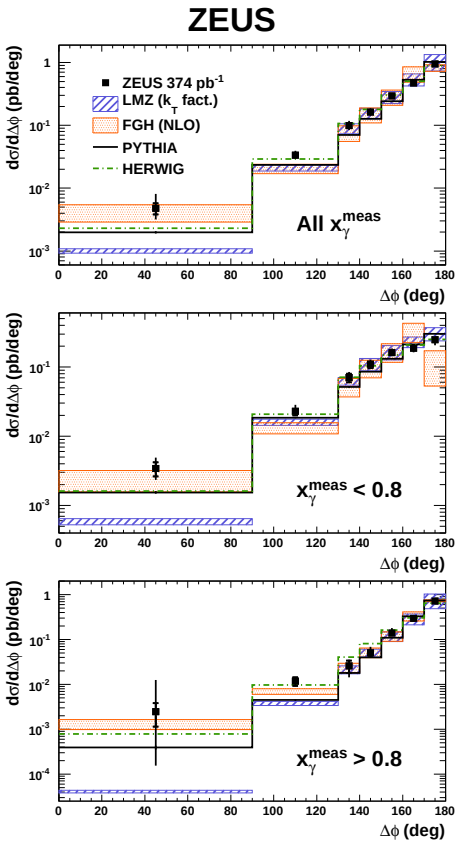

Figure 8: Distributions in azimuthal distance between photon and jet for the entire $x_\gamma^{\rm meas}$ range and for values less than and greater than 0.8, compared to calculations.